

to describe the extension of the September 10, 2000

September 10, 2020

Preprint submitted to Elsevier

dispersion properties [8]. The approach has also been successfully extended to include the effects of varying batohymetry and allow for the presence of dry beds [8]. It was demonstrated by Clamond and Dutykh [1] that the SGN also possesses a conservation reformulation and thus the technique described above for the SGN equations can be extended to the SGN. The success of this technique makes this an attractive option and would allow for an explicit, robust and conservative method for the SGN. Hence, the purpose of this paper is a description of the extension to the numerical scheme of Zoppou et al. [7] for the recently developed SGN [1].

107
pəmbar
n lymph

The generalised Serre-Green-Naghdi equations (SGN) were recently derived by Chamod and Dutykh [1]. They are a family of equations that generalise the classical Serre-Green-Naghdi equations (SGN) first derived by Serey [2] with the addition of two parameters β_1 and β_2 . The equations describe the behaviour of water waves in shallow water where the typical water depth h_0 is much smaller than the wavelength λ so that the shallowness parameter $\alpha = h_0/\lambda \ll 1$. The SGN are of particular interest to the wave modelling community as their dispersion relationship well approximates the dispersion relationship of the linear wave theory [3]. The choice of β values allows for the dispersion relationship of the SGN to be accurate up to $O(\alpha^2)$ terms [4]. Therefore, these equations provide a way to study the behaviour of water waves as higher powers of α are retained in the wave model.

In previous work we have developed and validated numerical methods for a conservative reformulation of the SGN [5, 6, 7, 8]. These numerical methods have all been based on the following approach; firstly solve an auxiliary elliptic equation containing only spatial derivatives, to obtain all the primitive variables in the conservation equation. Then evolve the remaining derivatives, to obtain a finite volume method. The benefit of this approach was the independence of the fundamental conservation properties of the SGN [8] and the

2. Introduction

10

We describe a numerical scheme for the recently derived generalized Serre-Green-Naghdi equations. This numerical scheme is an extension to the numerical scheme for the classical Serre-Green-Naghdi equations which solves an auxiliary elliptic equation to obtain all the necessary quantities and then solves the equations in conservation law form using a finite volume method. To validate the scheme we produced and implemented a second-order numerical version following the scheme. This numerical method is then validated using the known analytical solutions for particular members of the family of equations described by the generalized Serre-Green-Naghdi equations, in particular, a smooth solitary travelling wave and the dam-break problem. The numerical method is further validated for general members of this family of equations using forced solutions. The described method is conservative and thus the proposed numerical scheme.

1. Abstract

Jordan Pitt - jordan.pitt@anu.edu.au, Christopher Zoppou - christopher.zoppou@anu.edu.au, Stephen Roberts - stephen.roberts@gsau.edu.au

Numerical Scheme for the Generalised Serre-Green-Naghdi Model

To obtain the dispersion relation of the linearised SGN, (1) is first linearised by considering small waves on a mean flow depth h_0 and mean velocity of the flow u_0 . The dispersion relationship of the linearised SGN

The linear dispersion properties of water waves equations have been of particular interest [4, 11, 12], as the scope of wave modelling expands to include dispersive effects. Indeed, the gSGN are especially relevant due to their dispersion relation well approximating the dispersion relation given by the linear theory for water waves [3].

3.1. Dispersion Relation of the Linearised gSGN

Since (1) describes the conservation of mass, momentum and energy, when solutions are sufficiently smooth all equations hold simultaneously and the total amounts of all these quantities remain constant in time if the system is closed. This can be seen by integrating (1) over the domain, and observing that the temporal derivative of the spatial integrals of mass (h), momentum (uh) and energy (\mathcal{E}) is zero when there is no flux across the domain boundaries. This conservation property of the SGCN for h , uh and \mathcal{E} will be used to validate the numerical method and its solutions.

Equation (1) holds for all β values provided the solutions are sufficiently smooth. However, for particular β values, for example those corresponding to the SWE, it is possible to obtain non-smooth solutions for A and B that do not longer satisfy all three equations simultaneously [10]. Typically, since the mass and momentum equations are solved this results in dissipation of energy around discontinuities in solutions of the SWE. Conversely, when mass and energy equations are solved this results in dissipation of momentum and an incorrect shock speed for jump discontinuities.

When $\beta_1 = \beta_2 = 0$ these equations reduce to the SWWE with $\beta_1 = 2/3$ and $\beta_2 = 0$ the SGN are developed.

$$\left(\frac{x_Q}{\eta_Q} \frac{x_Q}{\eta_Q} \zeta_B \frac{\zeta}{1} + \frac{1}{1} \right) \zeta_B g \frac{\zeta}{1} + \frac{x_Q}{\eta_Q} \frac{x_Q}{\eta_Q} \varepsilon_B h \frac{\eta}{n} = 3$$

$$(P1) \quad \left[\frac{x_Q}{\eta_Q} \frac{x_Q}{\eta_Q} \frac{\zeta}{1} + \frac{\zeta}{\eta_Q} \frac{x_Q}{\eta_Q} \eta \right] B \zeta J - \left[\frac{\zeta x_Q}{n} n - \frac{\eta_Q x_Q}{n} \frac{\eta}{\eta_Q} - \frac{x_Q}{n} \frac{x_Q}{\eta_Q} \right] \eta J = 1$$

WHEI.E

$$(1c) \quad 0 = \left[\frac{x\varrho}{n\varrho} \frac{x\varrho}{\eta\varrho} \varepsilon \beta g h + \left(\frac{3}{1} + \left(\frac{x\varrho}{\eta\varrho} \frac{x\varrho}{\eta\varrho} \varepsilon \beta h \right) 1 + \frac{4}{1} \beta^2 h^2 \right) \frac{\eta\varrho}{\eta\varrho} \right] \frac{x\varrho}{\varrho} + \frac{\eta\varrho}{(\beta)\varrho}$$

$$(q_1) \quad 0 = \left(J_\varepsilon u \frac{\bar{z}}{1} + \varepsilon u^\beta \frac{\bar{z}}{1} + \varepsilon n u \right) \frac{x\varrho}{\varrho} + \frac{\varrho}{(n u)\varrho}$$

$$(I\!A) \quad 0 = \frac{x_Q}{(n\eta)Q} + \frac{\eta Q}{\eta Q}$$

The SGN were derived by Clamond and Dutykh [1] using a Lagrangian field theory approach. These equations generalize the SGN that describe a depth averaged approximation to the Euler equations, where $h(x, t)$ is the height of the free-surface of the water, $u(x, t)$ is the depth averaged horizontal velocity and g is the acceleration due to gravity. The SGN generalise the SWWE, the SGN equations by introducing two parameters β_1 and β_2 , that when fixed result in a particular member of this family of equations. In particular the family of equations captured by SGN contains the SWWE, the SGN, a family of regularised SWWE studied by Clamond and Dutykh [1] and a family of improved dispersion SGN equations studied by Clamond et al. [4]. The SGN describe the conservation of mass (h), momentum (uh) and energy (ϵ) for water waves subject to gravitational forces like so

3. Generalised Serre-Green-Naghdi Equations

After
of accuracy. Forced solutions are necessary to validate the numerical method for the more general members of this family of equations, because no analytic solutions are currently known. Together these validations demonstrate the capability of the numerical scheme to produce robust and accurate numerical methods.

$u_0 \pm \sqrt{gh_0} \sqrt{\beta_2/\beta_1}$. Therefore, u_\pm^p is monotonic and bounded at the limits of the domain, and thus bounded in addition to the monotonicity of u_\pm^p , when $k \rightarrow 0$ then $u_\pm^p \rightarrow u_0 \pm \sqrt{gh_0}$, whilst as $k \rightarrow \infty$ then $u_\pm^p \rightarrow u_0 - \sqrt{gh_0 f(h_0 k)}$, given the above properties of $f(h_0 k)$ under the initial assumptions $\beta_1 \geq \beta_2$ then u_\pm^p is monotone non-decreasing and u_\pm^p is monotone non-increasing when $\beta_1 \leq \beta_2$. Whereas when $\beta_1 < \beta_2$ then u_\pm^p is monotone non-decreasing and u_\pm^p is monotone non-increasing if $f(h_0 k)$ is monotone non-increasing if $\beta_1 \geq \beta_2$. Since $u_\pm^p = u_0 + \sqrt{gh_0 f(h_0 k)}$ and is greater than zero and thus $f(h_0 k)$ is monotone non-decreasing if $\beta_1 \leq \beta_2$. Whilst the derivative of the derivative is greater than zero and thus $f(h_0 k)$ is monotone non-decreasing if $\beta_1 \leq \beta_2$.

$$\frac{\partial (f(h_0 k))}{\partial (h_0 k)} = [\beta_2 - \beta_1] \frac{(\beta_1 (h_0 k)^2 + 2)}{4 (h_0 k)^2}.$$

is a monotone function over $h_0 k$. This can be seen by reformulating and taking the derivative with respect to $h_0 k$, to obtain that

$$f(h_0 k) = \frac{\beta_1 (h_0 k)^2 + 2}{\beta_2 (h_0 k)^2 + 2}, \quad \text{same solvers}$$

To demonstrate that the phase speeds are bounded, observe that when $\beta_1 \geq 0$, $\beta_2 \geq 0$ and $h_0 k \geq 0$ then to have bounded phase speeds then similar methods can be applied to solve the gSGN. Riemann solvers such as those of Krusen et al [14] to solve the SGN. Thus, if the gSGN can also be shown

Using phase speed bounds of the SGN Lee Metayer et al. [13] and Zoppou et al. [7] applied approximate only if used be the Metayer

$$u_\pm^g = \frac{\partial k}{\partial \omega} = u_0 \mp \sqrt{gh_0} \sqrt{\beta_1 h_0^2 k^2 + 2}, \quad (4b)$$

$$u_\pm^p = \frac{k}{\omega} = \frac{u_0 \mp \sqrt{gh_0}}{\sqrt{\beta_2 h_0^2 k^2 + 2}}, \quad (4a)$$

From the dispersion relation (2), the phase speed u^p and the group speed u^g can be derived as follows the physical phenomena.

SGN allow us to consistently compare the effect of the dispersion relationship on numerical solutions and thus terms and $O(\omega^6)$ terms. Since the β values allow us to alter the accuracy of the dispersion relationship, the term in the gSGN equations have a dispersion relationship that can be accurate up to $O(\omega^2)$ terms, $O(\omega^4)$ terms when $\beta_1 = \beta_2 + 2/3$ and $\beta_2 = 2/15$ [4]. Since $k = 2\pi/\lambda$, these powers of k correspond to a dispersion relation which is k^2 accurate for all β values, accurate to the k^4 term when $\beta_1 = \beta_2 + 2/3$ and accurate up to the k^6 term when $\beta_1 = \beta_2 + 2/3$ and $\beta_2 = 2/15$ [4].

$$u_\pm^g = (u_0 \mp \sqrt{gh_0}) k \mp \frac{4}{(\beta_2 - \beta_1)} \sqrt{gh_0} h_0^2 k^3 \mp \frac{32}{(3\beta_1^2 - 2\beta_2\beta_1 - \beta_2^2)} \sqrt{gh_0} h_0^4 k^5 + O(k^7). \quad (3b)$$

$$u_\pm^p = u_0 k \mp \sqrt{gh_0} \tanh(h_0 k) \mp \frac{6}{-1} \sqrt{gh_0} h_0^2 k^3 \mp \frac{360}{19} \sqrt{gh_0} h_0^4 k^5 + O(k^7) \quad (3a)$$

comparing their power series approximations provided below

The dispersion relation of the gSGN approximates the dispersion relationship of water, as can be seen by Duttyk [1] for the gSGN when $u_0 = 0$.

These waves are dispersive. This dispersion relation (2) is equivalent to the dispersion relation derived by Clamond and with wavenumber k . The dispersion relation has a positive and negative branch corresponding to the direction of these waves. These dispersion relations provide wave solutions of the linearised gSGN equations for waves which provides the angular frequency ω of travelling wave solutions of the form $\exp(i(kx - \omega t))$, as was done by Zoppou et al.

$$(2)$$

[7] to obtain

is then obtained by seeking travelling wave solutions of the form $\exp(i(kx - \omega t))$, as was done by Zoppou et al.

When $\beta_1 = 2/3$ then G is the same conserved quantity introduced for the SGN [7, 13, 15].

$$\frac{\partial G}{\partial t} + \frac{\partial}{\partial x} \left(uG + gh^2 - \beta_1 h^3 \frac{\partial u}{\partial t} - \frac{1}{2} \beta_2 gh^2 \left[h \frac{\partial x}{\partial t} + \frac{1}{2} \frac{\partial x}{\partial h} \right] \right) = 0$$

and thus (1b) can be written in conservation law form for G as

$$G = hu - \frac{2}{\beta_1} \frac{\partial x}{\partial t}$$

is obtained by introducing a new conserved quantity

derivative in the flux term of the momentum equation, which is difficult to treat numerically. This reformulation SGN [7, 13, 15] were reformulated. The purpose of this reformulation is to remove the mixed spatial-temporal Clamond and Dutykh [1] provided a reformulation of (1b) for the gSGN, in an analogous to the way the

3.2. Alternative Conservative Form of the gSGN

behind the rarefaction fan, and ahead of the shock due to the change of the chain of inequalities when $\beta_1 < \beta_2$. While for an illustrative example in Region 2 of the β plot we observe dispersive wave trains advancing fan. ~~While for an illustrative example~~, we observe a dispersive wave train between the shock and the rarefaction dispersion relationship respectively, we observe a dispersive wave train the SGN equations with $O(h_4)$ and $O(h_6)$ accuracy in the classical SGN equations and the improved dispersion SGN equations with $O(h_4)$ and $O(h_6)$ accuracy in the shock and the rarefaction fan for these non-dispersive wave models. For the dispersive wave models such as the shock and the rarefaction fan described well by the chain of inequalities (5) and (6) when $\beta_1 < \beta_2$. In particular, for the SWWE and the regularised SWWE $\beta_1 = \beta_2$ which results in a phase speed which is independent of h and thus a non-dispersive wave model. Consequently, we observe no wave train between $\beta_1 < \beta_2$. In particular, for the SWWE and the regularised SWWE $\beta_1 = \beta_2$ which results in a phase speed which is independent of h and thus a non-dispersive wave model. Consequently, we observe no wave train between $\beta_1 < \beta_2$. Ptit et al. [9] for the SGN. By comparing the numerical solution to its location in the β plot we can see that the behaviour of solutions is described well by the chain of inequalities (5) and (6) when $\beta_1 > \beta_2$ and the numerical solutions for the SWWE compare well to the study of the dam-break problems performed by Ptit et al. [9] for the SGN. By comparing the numerical solution to its location in the β plot we can see that the numerical solutions for the SWWE compare well to analytical solutions for the SWWE in Section 5.2, and the numerical solutions for the SWWE compare well to numerical solutions for the SWWE in Section 5.2, and the numerical solutions for the SWWE compare well to numerical solutions for the SWWE in Section 5.2. These numerical solutions are plotted at $t = 35s$ and are well resolved by the grid which contains 25600 cells. The numerical solution that describes the numerical scheme is valid for the dam-break problem in Section 5.2.

~~on solutions to the dam-break problem specified in Section 5.2. - deleted~~
~~numerical solution that demonstrates the effect of the β values and hence the different dispersion relationships between members of the SGN family given by the dispersion relationship. In addition to the middle plot of members of the SGN family, the improved SGN equations, obtaining $O(h_6)$ in the dispersion relationship one member of this family, the improved SGN equations, obtaining $O(h_6)$ in the dispersion relationship. In addition there is a family of equations that obtain $O(h_4)$ accuracy in the dispersion relationship with one particular All equations in the gSGN family are accurate up to $O(h_2)$ in the dispersion relationship (3). Furthermore, The regions and locations of important members of the gSGN in terms of β values is summarised in Figure 1. All equations in the gSGN family are accurate up to $O(h_2)$ in the dispersion relationship (3). Furthermore, the regions and locations of important members of the gSGN in terms of β values is valid for the regions.~~

~~to study using Region 1, although the numerical scheme is valid for the regions.~~

$$(9) \quad u_0 - \sqrt{gh_0} \sqrt{\frac{\beta_2}{\beta_1}} \leq u_+ \leq u_0 - \sqrt{gh_0} \leq u_0 \leq u_0 + \sqrt{gh_0} \sqrt{\frac{\beta_2}{\beta_1}} \leq u_+ \leq u_0 + \sqrt{gh_0}$$

When $\beta_2 > \beta_1$ the inequality chain becomes

$$(5) \quad u_0 - \sqrt{gh_0} \leq u_- \leq u_0 - \sqrt{gh_0} \sqrt{\frac{\beta_2}{\beta_1}} \leq u_0 \leq u_0 + \sqrt{gh_0} \sqrt{\frac{\beta_2}{\beta_1}} \leq u_+ \leq u_0 + \sqrt{gh_0}.$$

In addition, to the phase speed bounds we also have the following chain of inequalities when $\beta_1 \geq \beta_2$

~~be extended to the gSGN, the phase speeds are bounded.~~

for all β values provided that $\beta_1 = 0$ when $\beta_2 = 0$, otherwise the phase speeds are bounded. Consequently, the methods of Le Metayer et al. [13] and Zoppou et al. [7] for the SGN equations can be extended to the gSGN, the phase speeds are bounded.

because

Date: 10/09/2020 at 10:23am

File Name: gSGNpaper.tex

©Stere Notes by J. Put, C. Zoppou and S. Roberts.

$$\text{cup shape} \rightarrow \text{d}y_1 = \text{d}y_2 = 0 \text{ at } (0)$$

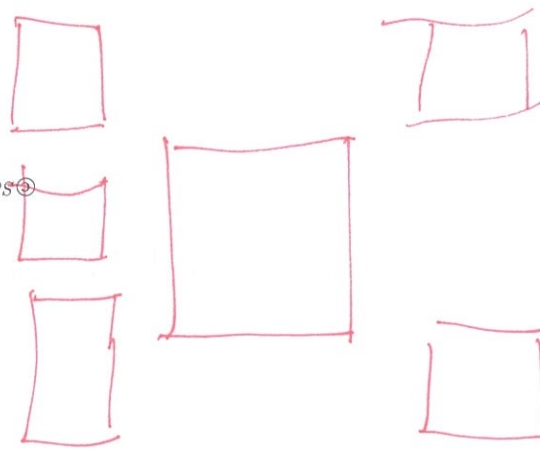
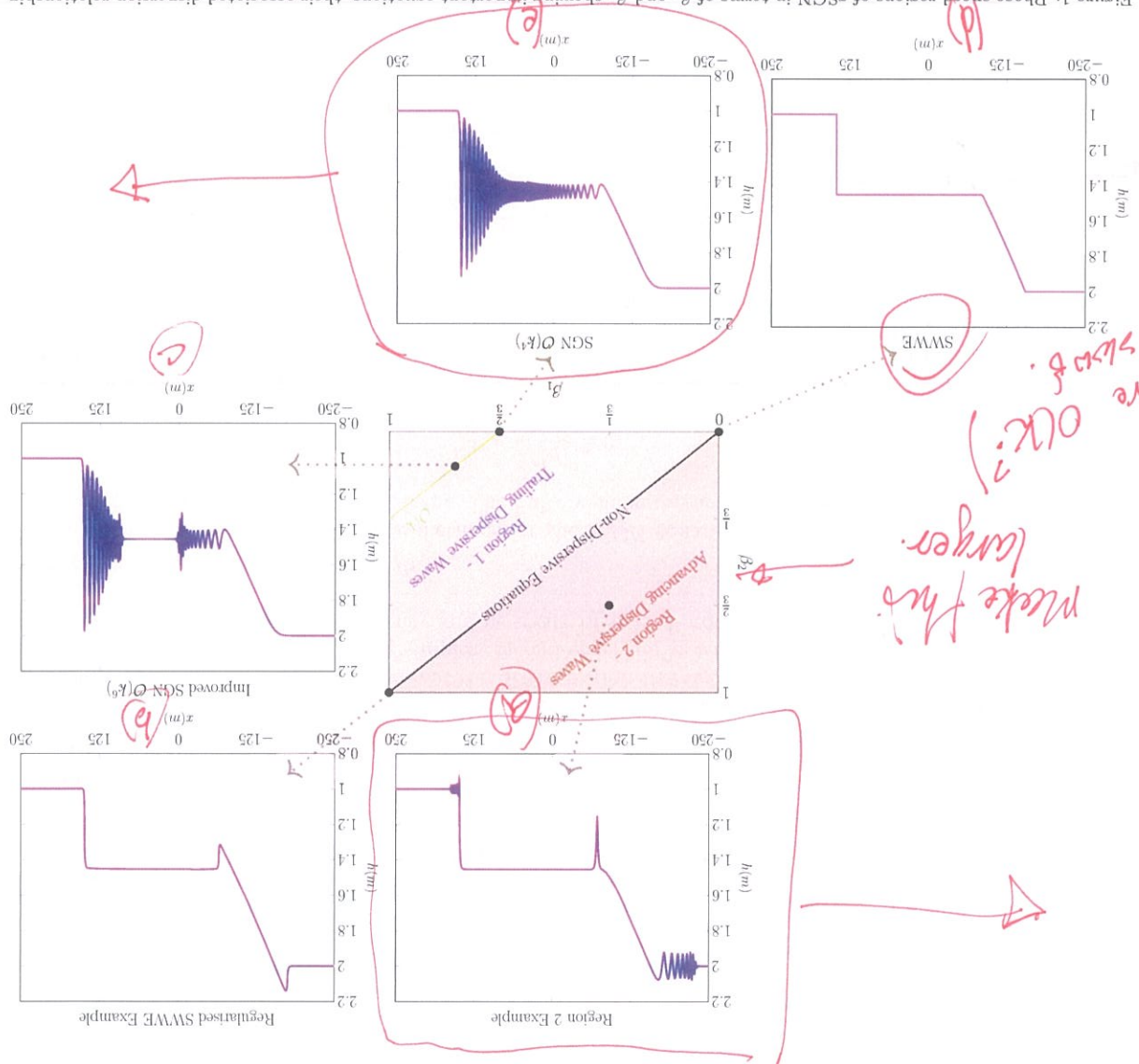


Figure 1: Phase speed regions of gSGN in terms of β_1 and β_2 showing important equations, their associated dispersion relationship accuracy (3) and an example numerical solution for the dam-break problem (27) solved using their respective β values.



In space only.

conserved quantities through time for equations in conservation law form (8). With the appropriate order of accuracy, then we have an explicit method for updating the cell average of the is the average flux of q across the cell edge from time t_n to t_{n+1} . Therefore, if $F_{j\pm 1/2}^n$ can be approximated

$$F_{j\pm 1/2}^n = \frac{1}{\Delta t} \int_{t_n}^{t_{n+1}} f(q(x_{j\pm 1/2}, t)) dt$$

is the average of q over the j th cell at time t_n and

$$\int_{x_{j-\Delta x/2}}^{x_{j+\Delta x/2}} q(x, t_n) dx = \frac{\Delta x}{1} \int_{x_{j-\Delta x/2}}^{x_{j+\Delta x/2}} q(x, t_n) dx$$

where

only first-order in time

$$q_{j+1}^n = q_j^n + \frac{\Delta x}{\Delta t} [F_{j+1/2}^n - F_{j-1/2}^n]$$

Integrating (8) over both space and time results in
 $x_{j-1/2}^n = x_0 + (f - \frac{c}{2}) \Delta x$ and $x_{j+1/2}^n = x_0 + (f + \frac{c}{2}) \Delta x$. Likewise the n th time step is given by $t_n = t_0 + n \Delta t$. In the finite volume method (8) is integrated over cells of fixed width Δx in space and over time steps of fixed length Δt . The midpoint of the j th cell is given by $x_j = x_0 + j \Delta x$ while the cell edges of the j th cell are given by $x_{j-1/2} = x_0 + (f - \frac{c}{2}) \Delta x$ and $x_{j+1/2} = x_0 + (f + \frac{c}{2}) \Delta x$. Likewise the n th time step is given by $t_n = t_0 + n \Delta t$. where q is a generic conserved quantity. This is the form of the gSGN equations after the reformulation (7).

$$(8) \quad 0 = \frac{\partial q}{\partial t} + \frac{\partial f(q)}{\partial x}$$

To solve the equations in conservation law form. The finite volume method solves equations of the form
 The heart of these hybrid finite volume methods for the gSGN equations is the finite volume method used
 4.1. Finite Volume Method and Discretisation

previous studies [7, 8] showing the sufficiency and necessity of second-order methods for the SGN equations.
 numerical technique and then describe the simplest second-order implementation of this scheme in detail. With a brief outline of the finite volume method and the discretisation therein. We then provide an overview of the any g values and the associated additional terms. We begin the description of the numerical scheme by giving

The proposed numerical scheme for the gSGN extends those previously published for the SGN [7, 13] to allow

4. Numerical Scheme

be solved numerically using the hybrid finite volume technique described by Zoppou et al. [7] for the SGN.
 Now that the gSGN are written in conservation law form and have a bound on the phase speeds, they can

$$(7c) \quad G = u_h - \frac{\beta_1}{\beta_2} \frac{\partial}{\partial x} \left(\frac{\partial}{\partial u} \varepsilon u_h \right)$$

with

$$(7b) \quad 0 = \left(\left[\frac{x \frac{\partial}{\partial x} G}{\beta_2 h^2} + \frac{2}{\beta_1 h^3} \frac{\partial}{\partial u} u_h - \frac{2}{\beta_2} \frac{\partial}{\partial x} g_h^2 \right] h \frac{\partial}{\partial u} \varepsilon + \frac{2}{\beta_2} \frac{\partial}{\partial x} \varepsilon \right) \frac{\partial}{\partial x} + \frac{\partial}{\partial t} + \frac{\partial}{\partial x} \left(u G \right) + \frac{\partial}{\partial x} \left(\beta_1 h^3 \frac{\partial}{\partial u} u_h - \frac{1}{\beta_2} \frac{\partial}{\partial x} g_h^2 \right)$$

$$(7a) \quad 0 = \frac{\partial}{\partial x} \left(\frac{\partial}{\partial u} \varepsilon u_h \right) + \frac{\partial}{\partial t} \left(\frac{\partial}{\partial u} \varepsilon u_h \right)$$

G. Thus the conservative gSGN are
 This reformulation, provides the gSGN in conservation law form for both h and the new conserved quantity

$$A(h_n, \mathcal{G}_n) = A_{-1} \mathcal{G}_n = u_n \leftarrow u_n. \quad (11)$$

Thus as desired we have

long as $h_n^j > 0$, which is true for all the problems of interest in this paper.

The finite difference approximation (10) can be solved with any matrix solver, for this method we use the explicit Thomas Algorithm [18]. This is an efficient method provided A is non-singular, which is the case as

with all other elements in A being zero.

$$\begin{aligned} A_{j,j+1} &= -\frac{\beta_1}{2} \left[\frac{\Delta x^2}{(h_n^j)^2} h_{n+1}^{j+1} - h_{n-1}^{j-1} \right] \\ A_{j,j} &= h_n^j + \beta_1 \left(\frac{\Delta x^2}{(h_n^j)^2} \right) \\ A_{j,j-1} &= -\frac{\beta_1}{2} \left[\frac{\Delta x^2}{(h_n^j)^2} h_{n+1}^{j-1} - h_{n-1}^{j-1} \right] \end{aligned}$$

where A is a tri-diagonal matrix with the sub-diagonal, diagonal and super-diagonal given by

$$u_n = A_{-1} \mathcal{G}_n \quad \text{numerical scheme.} \quad (10)$$

The second-order central finite difference approximation to (7c) can be written as

to accurately solve (7c).

Assuming that u is sufficiently smooth, then a second-order central finite difference approximation can be used value are equivalent up to second-order accuracy so that $q_n = b_n + O(\Delta x^2)$ for all the quantities of interest. To solve (7c) with h_n and \mathcal{G}_n to obtain u_n we use the observation that the cell average and the nodal

4.3.1. Step 1 - Solution of Elliptic Equation

the scheme.

To demonstrate the utility of this numerical scheme we present a simple second-order implementation, and then validate it in the following section. The description of this numerical method parts of steps described in Section 4.2 for simplicity and also to highlight the interchangingability of the different

[8] when $\beta_1 = 2/3$ and $\beta_2 = 0$. Additionally, when $\beta_1 = \beta_2 = 0$ the GSGN reduces to the SWVE, and this numerical scheme reduces to a finite volume method [17].

This numerical scheme produces the numerical methods of Le Metayer et al. [13], Zoppou et al. [7] and Pitt

method [16].

repetitions of Steps 1 and 2 to obtain a Strong Stability Preserving (SSP) Runge-Kutta time stepping method.

3. Since F is only first order accurate in time, Steps 1 and 2 are repeated a sufficient amount of times and

$$F(h_n, \mathcal{G}_n, u_n) \leftarrow h_{n+1}, \mathcal{G}_{n+1}.$$

2. Solve (7a) and (7b), using the finite volume method (9) with an approximate Riemann solver such as the one described by Kurganov et al. [14], to obtain h_n^j and \mathcal{G}_m^j at the next time step, like so

$$A(h_n, \mathcal{G}_n) \leftarrow u_n.$$

1. Solve (7c) using h_n and \mathcal{G}_n to obtain an approximation to u_n , which can be written

~~as~~ expressed as

~~G_n~~ are either known or provided as initial conditions.

The numerical scheme for the GSGN equations based on the finite volume method (9) then proceeds as follows. Begin at a generic n^{th} time step where the vectors of cell averages of the conserved quantities h_n and

q_n to be the vector of q_n^j values and q_n^j to be the vector of q_n^j values for all cells in the domain at time t_n .

We will now describe the numerical scheme, which uses the above finite volume formulation to solve (7a)

4.2. Overview

$$a_{+}^{\frac{z}{l}} = \max \left\{ 0, u_{-}^{j+1/2} + \max \left(1, \sqrt{\frac{\beta_1}{\beta_2}} g h_{+}^{j+1/2} \right) \right\} \quad (17)$$

$$a_{-\frac{\ell}{2}} = \min \left\{ 0, n_{-\frac{\ell}{2}}^{+} - \max \left(1, \sqrt{gh_{+\frac{\ell}{2}}} \right) \right\}, \quad (16)$$

where $a_+^{j+\frac{1}{2}}$ and $a_-^{j+\frac{1}{2}}$ are given by the Phase speed bounds and all quantities on the right hand side are computed at time t_n . Applying the Phase speed bounds (5) and (6) we obtain

$$\left[\begin{smallmatrix} \frac{\xi}{4} + f_b & -\frac{\xi}{4} + f_b \\ -\frac{\xi}{4} + f_b & \frac{\xi}{4} + f_b \end{smallmatrix} \right] \frac{\frac{\xi}{4} + f_v - \frac{\xi}{4} + f_v}{-\frac{\xi}{4} + f_v + \frac{\xi}{4} + f_v} + \frac{\frac{\xi}{4} + f_v - \frac{\xi}{4} + f_v}{\left(\frac{\xi}{4} + f_b \right) f \frac{\xi}{4} + f_v - \left(\frac{\xi}{4} + f_b \right) f \frac{\xi}{4} + f_v} = \frac{\frac{\xi}{4} + f_v}{u f}$$

In this numerical scheme the approximate remap solver described by Hiragano et al. [14] is used to calculate $F_{j+1/2}^n$. The major advantage of this scheme is that it only requires bounds on the phase speeds to calculate the flux $F_{j+1/2}^n$. Only the calculation of the flux term $F_{j+1/2}^n$ is demonstrated as the process to calculate the flux term $F_{j-1/2}^n$ is identical but with different cells. For y the flux is approximated by

4.3.3. Step 2 - Finite volume method - Flux approximation

generic

$$\frac{x\nabla}{\ell b - \ell + \ell} = \left[\frac{xQ}{bQ} \right]^{\ell/z}$$

order finite difference approximation at the cell edges is sufficient. We demonstrate this for $\mathcal{C}_{x+1/2}$ and a general quantity q

$j + 1$ gives rise to $q_{j+1/2}$ and $q_{j+3/2}$, all of which are required in the flux approximation.

This gives a reconstruction at the cell level for each cell edge, so cell j gives rise to $q_{j-1/2}$ and $q_{j+1/2}$ while cell

$$\min \text{mod}(a, b, c) = \begin{cases} 0 & \max(a, b, c) \leq 0, \\ \min(a, b, c) & \text{when } a < 0, b < 0, c > 0 \\ \max(a, b, c) & \text{when } a < 0, b > 0, c < 0 \\ \min(a, b, c) & \text{when } a > 0, b < 0, c < 0 \\ 0 & \text{otherwise} \end{cases} \quad (14)$$

The minmod function is defined as follows

$$\cdot \left(\frac{x\nabla}{\ell_B - 1 + \ell_B} \theta, \frac{x\nabla \zeta}{1 - \ell_B - 1 + \ell_B}, \frac{x\nabla}{1 - \ell_B - \ell_B} \theta \right) = \min_{\ell_B} f_\ell$$

WHERE

$$\text{and } \frac{\partial}{\nabla} \frac{b_{j+1/2}}{x} = b_{j+1/2} - b_j \quad (12)$$

We assume that these quantities are smooth and thus do not require limiting.

The finite volume method of Kurganov et al. [14] relies on approximations of all the terms in the spatial derivative of the flux at the cell edges $x^{\pm} = \frac{1}{2}$. Thus the following quantities require second-order approximations at the cell edges: $u, h, G, \partial u / \partial x, \partial h / \partial x, \partial^2 h / \partial x^2$. In this paper we are interested in reproducing solutions to either smooth analytic and forced solutions for all members of the gSGN. We are also interested in reproducing the discontinuous dam-break solution for only the SWWE where $G_1 = \beta_2 = 0$ and thus h, u and $G = uh$ need to be approximated. For this reason our gSGN solver uses approximations to u, h, G that allow for discontinuities and thus use limiting. Whereas the derivatives $\partial u / \partial x, \partial h / \partial x, \partial^2 h / \partial x^2$

4.3.2. Step 2 - Finite Volume Method - Reconstruction

Figure 1 has down-break problem for the after

For Step 2 there is no need to reconstruct the quantities inside the ghost cells because h , G and u are given. When $j < 0$ or $j > m - 1$.

$$A_{j,j-1} = 0 \quad A_{j,j} = 1 \quad A_{j,j+1} = 0 \quad (22)$$

the additional associated ghost cell values given by

Likewise the associated extended matrix A_m in (10) is the same as A when $0 \leq j \leq m - 1$ defined above with

$$G_u = [G_{m-1} \cdots G_0^{-1} G_0 \cdots G_{m-1} G_m \cdots G_{m+l-1}]^T \quad (21)$$

$$u_u = [u_{-l} \cdots u_{-1} u_0 \cdots u_{m-1} u_m \cdots u_{m+l-1}]^T \quad (20)$$

the ghost cells u_u and G_u like so

This boundary condition is applied to Step 1 by extending the matrix equation (10) to vectors containing ~~at least 2~~ ghost ~~from~~ from $m + l$ to $m + l - 1$. Since the numerical method has a maximum stencil that

extends 2 cells beyond the target cell, then l must be ~~at least 2~~ ≥ 2 . We have an additional l cells side of it so that we have the left ghost cells $-l, -l + 1, \dots, -1$ and the right ghost cells $m + 1, \dots, m + l - 1$. Since the numerical method has a maximum stencil that boundary we have an additional l cells either side of it so that we have the left ghost cells $-l, -l + 1, \dots, -1$ using ghost cells over which the values of h , G and u are known. Thus in addition to the m cells inside the For the purposes of the validation below and for simplicity, we have applied Dirichlet boundary conditions

4.4. Boundary Conditions

obtaining a stable fully second-order method for solving (7).

$$\begin{aligned} h_{n+1}, G_{n+1} &= \frac{2}{1} \left(h_n + \frac{2}{1} \left(\frac{2}{1} \left(G_n + G_{n+1} \right) \right) \right) \\ h_{(2)}, G_{(2)} &= F \left(h_{(1)}, G_{(1)}, A \left(h_{(1)}, G_{(1)} \right) \right) \\ h_{(1)}, G_{(1)} &= F \left(h_n, G_n, A \left(h_n, G_n \right) \right) \end{aligned}$$

of A , (11) and F , (19)

To arrive at a fully second-order method, we repeat Steps 1 and Steps 2 according to the second-order SSP Runge-Kutta method [16]. Doing this we obtain the following scheme making use of the above implementation combining both Steps 1 and Steps 2, provides a spatially second-order scheme with first-order time stepping.

4.3.4. Step 3 - Runge-Kutta Time Stepping

as desired.

$$F(h_n, G_n, u_n) = \frac{\partial}{\Delta t} \left[F_n^{j+1/2} - F_{n-1}^{j-1/2} \right] \leftarrow h_{n+1}, G_{n+1} \quad (19)$$

and thus employ (9) to obtain h_{n+1} and G_{n+1} resulting in

Since the reconstructions were given above for all these quantities, we can approximate $F_n^{j+1/2}$ using (15) script.

where the derivatives are assumed to be smooth across the cell edge, and thus do not require different super-

$$\begin{aligned} f(G_{\mp}^{j+1/2}) &= u_{\mp}^{j+1/2} G_{\mp}^{j+1/2} + \frac{2}{\beta} \left(h_{\mp}^{j+1/2} \right)^2 - \beta_1 \left(h_{\mp}^{j+1/2} \right)^2 \\ &\quad - \frac{1}{2} \beta_2 g \left(h_{\mp}^{j+1/2} \right)^2 + \frac{1}{2} \left(\frac{\partial g}{\partial h} \right) \left(h_{\mp}^{j+1/2} \right)^2 \end{aligned} \quad (18)$$

For the evolution of G equation (7b) we have

$$f \left(h_{\mp}^{j+\frac{1}{2}} \right) = u_{\mp}^{j+1/2} h_{\mp}^{j+1/2}.$$

cell respectively. From the continuity equation (7a) we have

The flux functions $f(q_{\pm}^{j+\frac{1}{2}})$ and $f(q_{\mp}^{j+\frac{1}{2}})$ are evaluated using the reconstructed values of the j_{th} and $(j+1)_{th}$ choice of G values.

where the max $\left(1, \sqrt{\beta_2/\beta_1} \right)$ accounts for the different phase speed bounds (5) and (6), which depend on the

out in balance

where

The analytic solutions used to validate the numerical method, are the solitary travelling wave solution of the SWWE demonstrated the robustness of the method in the presence of steep gradients. The dam-break solution of the SWWE, the solitary travelling wave solution is a smooth travelling wave solution, that assesses the balance of the non-linear and dispersive terms in the gSGN. Whereas the dam-break solution of the SWWE, the solitary travelling wave solution is a smooth travelling wave solution of the SWWE demonstrates the robustness of the method in the presence of steep gradients.

5.2. Analytic Solutions

$$\text{equation} \quad (25)$$

$$C_1(q_0, q_n) = \left\{ \begin{array}{l} |C(q_0) - C(q_n)|, \quad |C(q_0)| = 0 \\ \frac{|C(q_0)|}{|C(q_0) - C(q_n)|}, \quad |C(q_0)| < 0 \end{array} \right.$$

equation

For a quantity q with a vector of its values at the n^{th} time step q_n , the total amount of the quantity is approximated by $C(q_n)$. The method for this is the same as the method described by Zoppou et al. [7], which has a higher order of accuracy than the numerical method for the gSGN. Using the numerical approximation to the total amounts, the conservation error is obtained using

where the time-step superscripts were suppressed for simplicity.

want to solve

$$(24)$$

$$L_2(q, q_*) = \left(\sum_{j=1}^J \frac{(q_j - q_*^j)^2}{2} \right)^{1/2}$$

For a quantity q with a vector of its analytic or forced solution at the cell midpoints q and the numerical solution at the cell midpoints q_* , the discrete non-dimensional L_2 norm is

Comparing them using a measure called C_1 .

be measured by numerically approximating the energy in the initial conditions and the numerical solution will be measured by forced solution using the L_2 norm. While the conservation properties of the numerical method will analyse of convergence will be the relative distance between the numerical solution and the equivalent analytical or forced solution.

To validate the produced numerical solutions we make use of measures of convergence and conservation.

convergence of solution of

5.1. Convergence and Conservation Measures

The example numerical method described above is validated using analytic solutions for particular q values that correspond to the gSGN and the SWWE as well as a forced solution. Together these tests demonstrate the ability of the method to reproduce analytic solutions to important members of the gSGN family, as well as assessing the accuracy of the numerical method's approximation to all terms of the gSGN.

5. Validation

where $a_{j+1/2}^+$ are the phase speed bounds used in the flux approximation (17) and $0 \leq Cr \leq 1$ is the Courant number.

$$(23)$$

$$\Delta t \leq \frac{\max_j \{ a_{j+1/2}^+ \}}{\Delta x} Cr$$

To ensure the stability of the finite volume method (9) the Courant-Friedrichs-Lowy (CFL) condition [19] is used. The CFL condition is necessary for stability and ensures that time steps are small enough so that information is only transferred between neighbouring cells. For the gSGN equations the CFL condition is

4.5. Courant-Friedrichs-Lowy Condition

The conservation error C_1 (25) of the numerical solutions as Δx varies is given in Figure 4. This conservation measure demonstrates that the finite volume method conserves h and G up to round-off error, which accumulates little distinction and is second-order accurate.

Example numerical solutions for h , u and G with $\Delta x = 400/(100 \times 2^6) \approx 0.06m$ are plotted in Figure 2. These examples demonstrate that the numerical solutions can reproduce the analytic solutions well.

¹ Numerical experiments [7, 8].

The numerical solution was solved over the domain [-200m, 200m] from $t = 0$ until $t = 30$ s. To ensure that the SGN solution is recovered, $D_1 = -2/3$ and $D_2 = 0$. The spatial resolution was varied like so $\Delta x = 400/(100 \times 2^l)$, where l was increased from 0 to 12. To satisfy the CFL condition (23) the time step width $\Delta t = \Delta x/(2\sqrt{g(a_0 + a_1)})$ [8] was chosen. The limiting parameter $\theta = 1.2$, was chosen to match previous calculations due to gravity at the initial surface, $g = 9.81\text{m/s}^2$.

This travelling wave solution is maintained due to a balance between the dispersive terms and the non-linear terms in the momentum equation (1b). This balance results in a solitary wave that is advected with a constant speed without a change in shape. Validating the numerical solutions for the SGN solver using this solution tests the balance between these terms in (1b), and allows us to verify the method's conservation of energy as the solution is smooth. To enable a comparison between the numerical method and the SGN solver of Zoppou et al. [7] and Pitt [8], the chosen solitary travelling wave parameters were $a_0 = 1\text{m}$ and $a_1 = 0.7\text{m}$ and the acceleration due to gravity at the earth's surface, $a = 9.81\text{m}^2/\text{s}^2$ was used.

$$\underline{(1v + 0v) \delta} \wedge = 0$$

and

$$k = \frac{2a_0 \wedge a_1}{\sqrt{3a_1}}$$

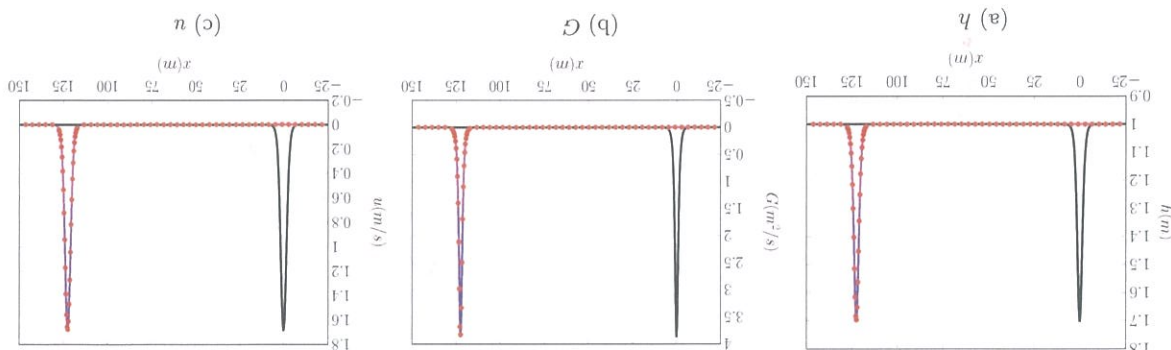
where

$$\left(\frac{(\tau^* x)q}{0d} - 1 \right) c = (\tau^* x)n$$

$$h(x,t) = a_0 + a_1 \operatorname{sech}^2(k(x - ct)), \quad (26a)$$

When $\beta_1 = 2/3$ and $\beta_2 = 0$ the SGN are equivalent to the SGN which admit the following travelling wave solution [20]

Figure 2: Plot of comparing initial (—), analytic solution (—), and numerical solution with $\Delta x \approx 0.06\text{m}$ (●) at $t = 30\text{s}$.



equation

for the SGN

These results agree well with the numerical solutions of Pitt [8], who compared various numerical methods indicating that the peak is travelling at the correct speed to cell width accuracy. This diffusion becomes negligible when Δx is small, and for the lowest Δx value we observe that $c_- < c_+$, this diffusion is large, both the upper and lower bounds on the wave speed are below the analytical value c given by (26) in Figure 5. This figure demonstrates the diffusion of the numerical scheme, as when Δx is large, both the upper and lower bounds on the wave speed are compared to the analytical value c given by (26) in Figure 5. These upper and lower bounds are compared to $0.5\Delta x/\tau$ and the upper bound is $c_+ = (x_{peak\ cell} + 0.5\Delta x)/\tau$. The lower bound is $c_- = (x_{peak\ cell} - 0.5\Delta x)/\tau$ and the wave problem where the lower bound is $c_- = (x_{peak\ cell} - 0.5\Delta x)/\tau$ and the upper bound is $c_+ = (x_{peak\ cell} + 0.5\Delta x)/\tau$.

By locating the cell on which h_u achieves its maximum, we can provide an upper and lower bound for the convergence in Δx .

Figure 4: Conservation plot for h (□), G (○), u_h (Δ) and u (×) as Δx varies.

SGN equation

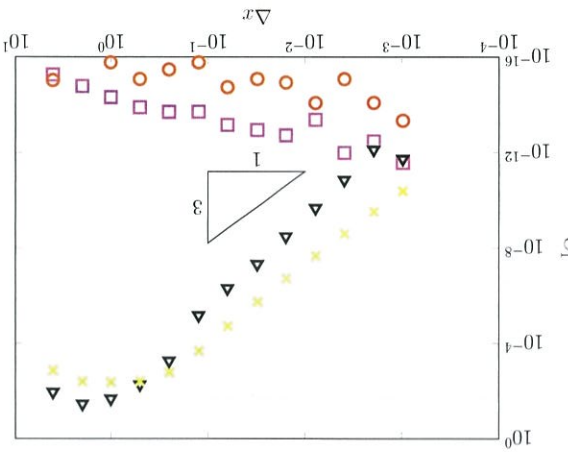
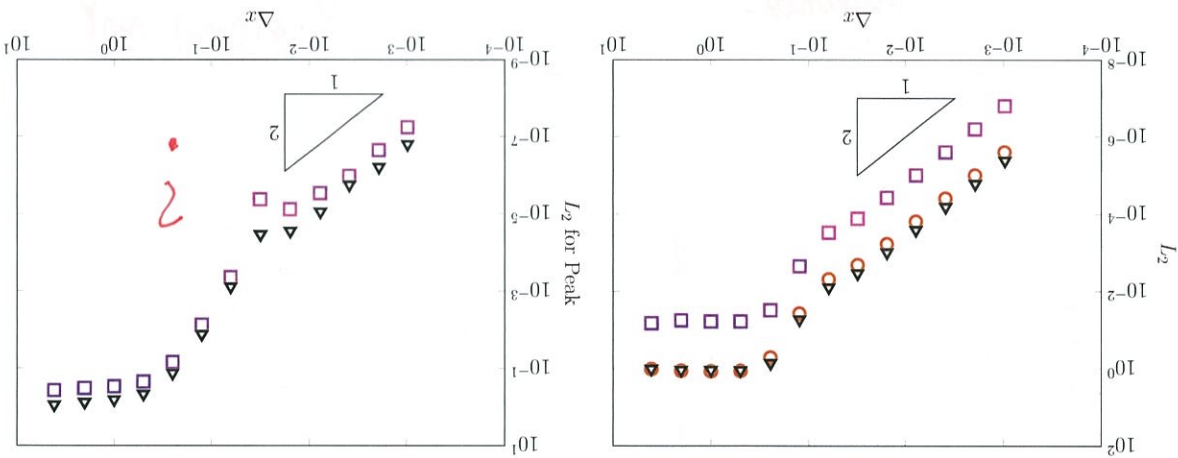


Figure 3: Convergence plots for h (□), G (○) and u (Δ) as Δx varies.

(b) Peak Only

(a) Whole Domain



the discontinuity or entropy shockwave

The initial conditions as well as the analytic solution are discontinuous. Due to the discontinuities the solutions to the initial conditions are not unique, as solving any pair of the 3 conservation equations (1), gives

$$S_0 = \frac{h_2 - h_1}{2h_2} (\sqrt{gh_0} - \sqrt{gh_2}) \quad (29c)$$

$$u_2 = 2(\sqrt{gh_1} - \sqrt{gh_2}), \quad (29b)$$

$$h_2 = \frac{h_0}{2} \left(1 + \sqrt{1 + 8 \left(\frac{\sqrt{gh_0}}{2h_2} (\sqrt{gh_1} - \sqrt{gh_2}) \right)^2} \right) \quad (29a)$$

solving

The constant state values h_2 and u_2 and the shock speed S_0 can be calculated for any initial conditions by

$$\begin{cases} u(x,t) \\ h(x,t) \end{cases} = \begin{cases} 0 & x \leq S_0 t \\ \frac{h_0}{2} & x \leq S_0 t \\ \frac{h_1}{2} & x \leq S_0 t \\ h_0 & x \geq S_0 t \end{cases} \quad (28b)$$

$$\begin{cases} u(x,t) \\ h(x,t) \end{cases} = \begin{cases} 0 & x \leq S_0 t \\ \frac{h_0}{2} & x \leq S_0 t \\ \frac{h_1}{2} & x \leq S_0 t \\ h_0 & x \geq S_0 t \end{cases} \quad (28a)$$

by

The solution to the dam-break problem using the conservation of mass and momentum equations is given

$$G(x, 0) = 0. \quad (27c)$$

$$0 = u(x, 0) \quad (27b)$$

$$\begin{cases} 0 & x \leq 0 \\ h_0 & 0 > x \end{cases} = u(x, 0) \quad (27a)$$

possess an analytic solution to the dam-break problem given by the initial conditions

When $\beta_1 = \beta_2 = 0$ the SGN equations reduce to the SWWE and consequently $G = uh$. The SWWE

5.2.2. SWWE ($\beta_1 = \beta_2 = 0$) - Dam-break Solution

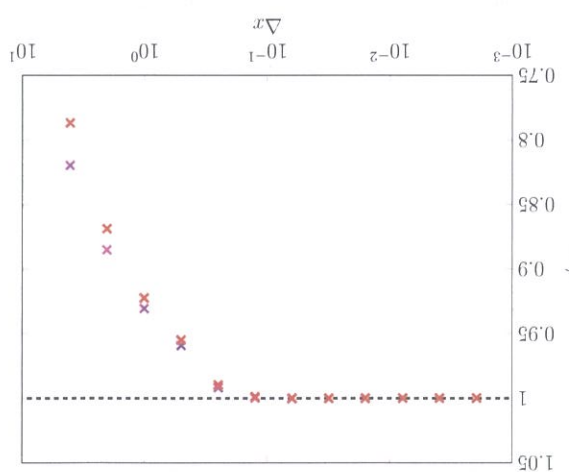


Figure 5: Plot of c^*/c (red 'x') and the analytic value (—) as Δx varies.

solve it to E
this is not what you

at the shock

These results demonstrate that the analytic solution of the SWWE has been accurately reproduced by the numerical method.

in the solution; therefore; the shock is resolved.

and x_{upper} provide a bound for the true location of the shock. Additionally it demonstrates that as Δx decreases the numerical solutions are better resolving the shock. Additionally it demonstrates that as Δx calculated and compared to the analytic value S_2 given by (29c) in Figure 8. This figure demonstrates that as calculated for the shock speed $S_{2+} = x_{lower}/t$ and the upper bound for the shock $S_{2-} = x_{upper}/t$ were lower bound this was achieved by finding the first cell with $h_1 \leq h_1 + \frac{9}{10}(h_2 - h_1)$ at the final time which we call x_{lower} , and for the upper bound this was found by finding the first cell with $h_1 \leq h_1 + \frac{9}{10}(h_2 - h_1)$ at the final time which we call x_{upper} . Consequently, the bound for the shock speed $S_{2+} = x_{lower}/t$ and the upper bound for the shock $S_{2-} = x_{upper}/t$ were

in the solution; therefore; the shock is resolved.

and upper bounds for the shock speed in the numerical solution. For the lower bound this was accomplished by finding the first cell with $h_1 \leq h_1 + \frac{9}{10}(h_2 - h_1)$ at the final time which we call x_{lower} , and for the upper bound this was found by finding the first cell with $h_1 \leq h_1 + \frac{9}{10}(h_2 - h_1)$ at the final time which we call x_{upper} .

To further justify the ability of the method to resolve the discontinuous analytic solution, I have found lower and upper bounds for the shock speed in the numerical solution. Given that this solution contains a discontinuity these are good conservation results.

at the shock

To recover first-order accuracy. Given that this solution contains a discontinuity these are good conservation to recover first-order accuracy. However, when accounting for the lack of energy conservation by using E^* we are able to improve as Δx decreases. However, this can be seen as the conservation error of E does not

at the shock

Energy is not conserved by the analytic solution, and this can be seen as the conservation error of E does not increase as Δx increases. Since $G = uh$, this means that h is also conserved up to round-off error

at the shock

discontinuities the quantities h and G are conserved up to round-off error, leading to their conservation in Figure 7b. This figure demonstrates that due to the finite volume method even in the presence of

at the shock

error for mass, momentum and energy as calculated normally and the new corrected energy are all compared total energy in the numerical solution to total energy in the analytic solution at the final time. The conservation of total energy by comparing the energy by comparing the total energy in the numerical solution to the total energy in the analytic solution is no longer valid. Hence, we introduce a new measure E^* which measures the conservation error of the energy by comparing the

at the shock

comparing the total energy in the numerical solution at the final time to the initial conditions is no longer valid. Since we solved equations for h and G , these quantities are conserved in the analytical solutions however, E is no longer conserved and energy is lost as the shock propagates. Therefore,

at the shock

analytic solutions with the total energy is lost at the final time to the initial conditions is no longer valid.

at the shock

Since the analytic solution contains all three conservation laws for h , G and E are not all

at the shock

robust in the presence of steep gradients and accuracy from discontinuities, as desired.

at the shock

The presence of discontinuities in the numerical solution makes it difficult to assessing convergence of the numerical solution. To circumvent these issues, the convergence measure $\frac{\|G - G_n\|}{\|G\|}$ is plotted in Figure 7a. This figure demonstrates that the scheme

at the shock

the numerical and analytic solutions for the constant region between the rarefaction fan and the shock. This

at the shock

modifies convergence measure as Δx varies in Figure 7a. This figure demonstrates that the scheme

at the shock

reduces the error in the numerical solution at the final time to the initial conditions is no longer valid.

at the shock

Figure 6 shows the spatial resolution $\Delta x = 500/(100 \times 2^6) \approx 0.15m$ and the analytic

at the shock

solutions for h , G and u at the final time are plotted in Figure 6. These figures demonstrate that the method

at the shock

is robust in the presence of steep gradients and accuracy from discontinuities, as the basis of the numerical

at the shock

method. Figure 6 compares the initial condition with the spatial resolution $\Delta x = 0.15m$ and the analytic

at the shock

mass and momentum equations, as these equations are the basis of the numerical method.

at the shock

solutions with similar structures but different shock speeds. The solution presented above is solution of the

at the shock

numerical experiments were run for the dam-break problem with $h_0 = 2m$ and $h_1 = 1m$. The

at the shock

number of numerical experiments were run for the dam-break problem with $h_0 = 2m$ and $h_1 = 1m$. The

at the shock

domain of the solution was $[-250m, 250m]$ with a final time of $t = 35s$. The spatial resolution was varied like so

at the shock

$\Delta x = 500/(100 \times 2^6)$ where l was increased from 0 to 12. To satisfy the CFL condition (23) the time step length

at the shock

$\Delta t = \Delta x / (2\sqrt{g_0})$ was used. The limiting parameter $\theta = 1.0$ and the acceleration due to gravity $g = 9.81m^2/s^2$

at the shock

were used.

at the shock

Figure 6: Comparison of initial (—), analytic solution (—), and numerical solution with $\Delta x \approx 0.15m$ (●) at $t = 35s$.

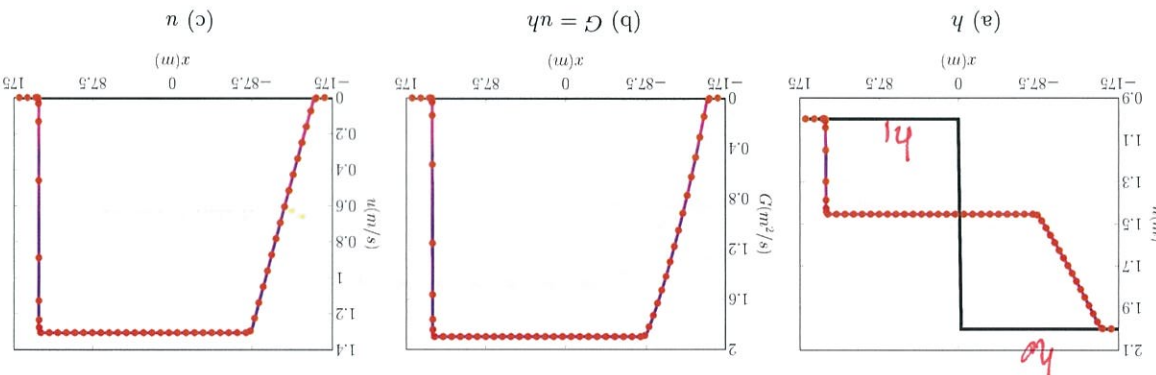


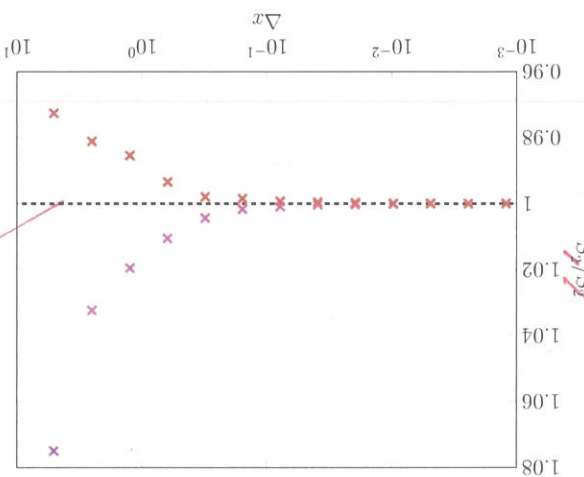
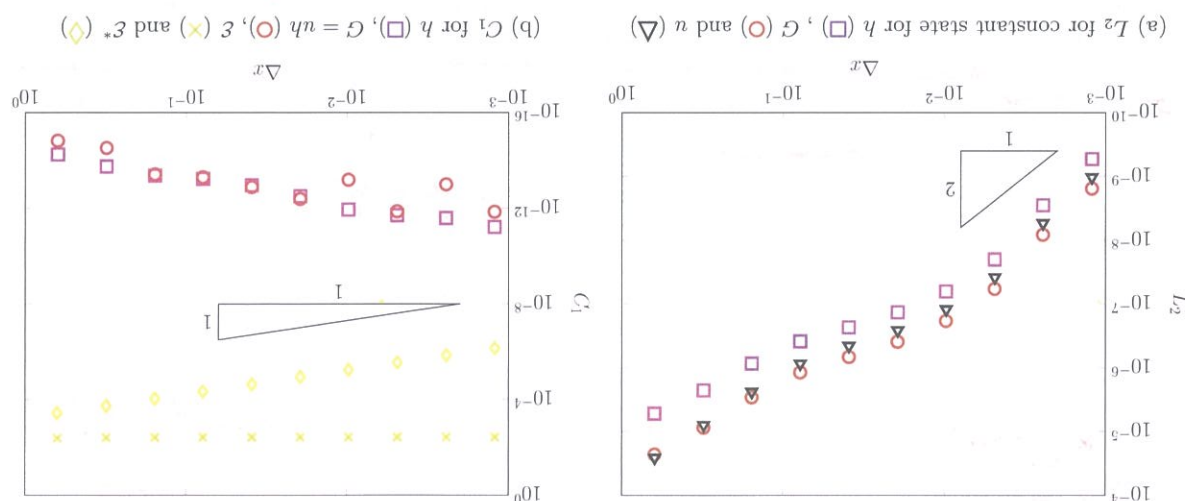
Figure 8: Plot of $S_{\lambda}^{2,+}/S_2(x)$, $S_{\lambda}^{1,-}/S_2(x)$ and analytical value (—) as Δx varies.

Figure 7: Convergence and conservation plots.



all time

Figure 10 demonstrates the convergence of the numerical scheme as Δx decreases. All quantities of interest are converging at the expected second-order. Since the right-hand-sides of (30) are evaluated analytically, the observed error is caused by the numerical method. Therefore, these results demonstrate that the scheme is second-order for all terms in the gSGN.

Figure 9 compares an example numerical solution at the final time for h , G and u with $\Delta x = 200/(100 \times 2^5) \approx 0.06m$ with the analytical solution. These example solutions demonstrate that the numerical method is able to reproduce the forced solution well, validating the numerical methods approximation to all terms in (7).

Figure 9 compares an example numerical solution at the final time for h , G and u with $\Delta x = 200/(100 \times 2^5) \approx 0.06m$ with the analytical solution. These example solutions demonstrate that the numerical method is able to

are smooth, such reconstruction is not necessary.

forced solutions the limiting on the reconstruction on h , u and G was removed. Because these forced solutions are smooth, such reconstruction is not necessary.

all time

$\Delta t = \Delta x / (2 [a_4 + a_2 + \sqrt{g(a_0 + a_1)}])$. The acceleration due to gravity $g = 9.81m^2/s$ was used. For the spatial resolution was varied like so $\Delta x = 200/(100 \times 2^k)$, while the CFL condition was satisfied by setting $\Delta t = 10s$. The numerical solution were produced over the domain $[-100m, 100m]$ with a final time of $t = 10s$.

The multiple G values were tested we will be focusing on $a_6 = 2/15 + 2/3$ and $a_7 = 2/15$ below.

The particular parameter values $a_0 = 1$, $a_1 = 0.5$, $a_3 = 20$ and $a_4 = 0.3$ were chosen in this investigation, include all the terms in the gSGN when assessing the numerical method.

since it requires the derivatives to be defined in the classical strong sense. This ensures that the forced solutions not constant over the whole domain. Smoothness is necessary for the current description of the forced solutions, at a constant speed a_2 . This forced solution was chosen because it is smooth and because the terms in (30) are

where G^* is given by (7c), were used. These forced solutions describe Gaussian bumps in h and u that travel

$$\beta_2(x, t) = a_7 \quad (31d)$$

$$\beta_1(x, t) = a_6 \quad (31e)$$

$$h^*(x, t) = a_0 + a_1 \exp\left(\frac{(x - a_2 t)^2}{2 a_3}\right) \quad (31f)$$

$$u^*(x, t) = a_4 \exp\left(\frac{(x - a_2 t)^2}{2 a_3}\right) \quad (31g)$$

why $L = i$

The following forced solution equations.

gSGN equation (30) with the same convergence properties as the underlying numerical method for the gSGN method with the analytic expressions for the right-hand-side, produces a method that approximates the forced hand-side of these modified equations are approximated by the numerical method, combining the numerical hand-side of the above validation using analytic solutions. Since the left problems were $\beta_2 \neq 0$ which were not covered in the above validation using analytic solutions. In particular, the method for a larger class of problems than permitted by currently known analytic solutions. The problem the equations are satisfied for any chosen h^* , u^* and G^* , assuming G^* appropriately satisfies (7c). Since these

$$\begin{aligned} \partial G^* &+ \frac{\partial}{\partial x} \left(u^* G^* + \frac{g(h^*)^2}{2} - \beta_1(h^*)^3 \partial_u u^* - \frac{1}{2} \beta_2 g(h^*)^2 \left[h^* \partial_x^2 h^* - \frac{1}{2} \partial_h h^* \partial_h^2 h^* \right] \right) = 0 \\ &= \left(\frac{\partial}{\partial t} + \frac{\partial}{\partial x} \left(u G + \frac{g h^2}{2} - \beta_1 h^3 \partial_u \partial_u - \frac{1}{2} \beta_2 g h^2 \left[h^* \partial_x^2 h^* + \frac{1}{2} \partial_h h^* \partial_h^2 h^* \right] \right) \right) \end{aligned} \quad (30a)$$

$$\frac{\partial}{\partial t} + \frac{\partial}{\partial x} \left(u \partial_t h^* + \frac{\partial}{\partial x} (u h^*) \right) = \frac{\partial}{\partial x} + \frac{\partial}{\partial t} \left(\frac{\partial}{\partial x} (u h^*) \right) \quad (30b)$$

that's known

To generate a forced solution the forced gSGN are considered and thus the shown analytic solutions do not assess the numerical methods accuracy for the β_2 terms. Hence, to demonstrate the validity and versatility of the method to solve the gSGN for other G values, forced solutions are necessary. It is vital for the gSGN equations in particular because for the G values tested above β_2 is zero, and thus the shown analytic solutions do not assess the numerical methods accuracy for the β_2 terms. Hence, to demonstrate the validity and versatility of the method to solve the gSGN for other G values, forced solutions are necessary. It is vital for the gSGN equations in particular because for the G values tested above β_2 is zero,

There are no currently known analytic solutions to the gSGN equations for other G values. Hence, to

5.3. Forced Solutions

Figure 10: Convergence plot of h (□), G (○), u (Δ) for the forced solutions for various Δx values.

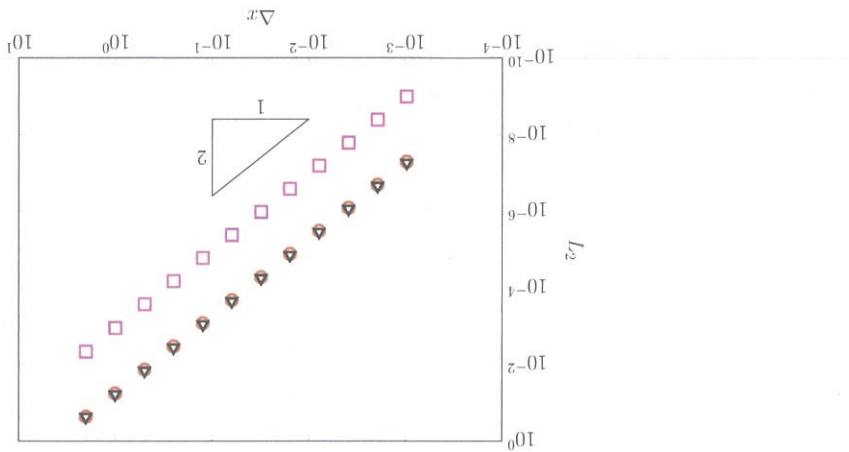
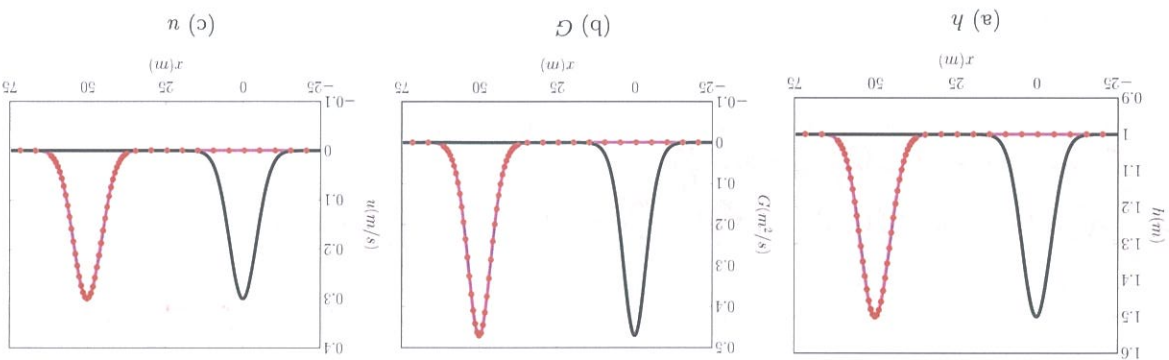


Figure 9: Example plots of initial conditions (—), analytic solution (—), and numerical solution with $\Delta x \approx 0.06m$ (●).



Section 11

A modified version of the numerical scheme for the SGN outlined by Zoppou et al. [7] was used to solve the SGN [1, 4]. This numerical scheme for the SGN was validated by describing a fully second-order order implementation as an example numerical method. This example numerical method was validated against analytical solutions of the SGN and SWVE and forced solutions. The analytic solutions demonstrate that the SGN solver accurately reproduces important members of the SGN family of equations whilst conserving the free parameters, B_1 and B_2 . The SGN method described above is the first validated numerical method for the free the SGN.

6. Conclusion

6. Conclusion

unförbund

- [3] G. B. Whitham. Non-linear dispersion of water waves. *Journal of Fluid Mechanics*, 27(2):399–412, 1967.

[4] D. Clamond, D. Dutykh, and D. Mitsotakis. Conservation laws modified Serre-Green-Naghdi equations with improved dispersion characteristics. *Communications in Nonlinear Science and Numerical Simulation*, 45: 245–257, 2017.

[5] C. Zoppou. Numerical Solution of the One-dimensional and Cylindrical Serre Equations for Rapidly Varying Free Surface Flows. PhD thesis, Australian National University, Canberra, ACT 2600, Australia, 2014.

[6] C. Zoppou, S.G. Roberts, and J. Pitt. A solution of the conservation law form of the Serre equations. *The Australian and New Zealand Industrial and Applied Mathematics Journal*, 57(4):385–394, 2016.

[7] C. Zoppou, J. Pitt, and S. Roberts. Numerical solution of the fully non-linear weakly dispersive Serre equations for steep gradients. *Applied Mathematical Modelling*, 48:70–95, 2017.

[8] J.P.A. Pitt. *Simulation of Rapidly Varying and Dry Bed Flow using the Serre Equations solved by a Finite Element Volume Method*. PhD thesis, Australian National University, Mathematical Sciences Institute, Canberra, ACT 2600, Australia, 2019.

[9] J.P.A. Pitt, C. Zoppou, and S.G. Roberts. Behaviour of the Serre equations in the presence of steep gradients revisited. *Wave Motion*, 76(1):61–77, 2018.

[10] Y. Pu, R.L. Pego, D. Dutykh, and D. Clamond. Weakly singular shock profiles for a non-dispersive regularization of shallow-water equations. *Communications in Mathematical Sciences*, 16:1361–1378, 2018.

[11] A. G. Filiaggi, M. Kazolea, and M. Ricchituto. A flexible genuinely nonlinear approach for non-linear wave propagation, breaking and run-up. *Journal of Computational Physics*, 310:381–417, 2016.

[12] J.S.A. do Carmo, J.A. Ferreira, and L. Pinto. On the accurate simulation of nearshore and dam break problems involving dispersive breaking waves. *Wave Motion*, 85:125 – 143, 2019.

[13] O. Le Metayer, S. Gavrilyuk, and S. Hank. A numerical scheme for the Green-Naghdi model. *Journal of Computational Physics*, 229(6):2034–2045, 2010.

- [14] A. Kurganov, S. Noelle, and G. Petrova. Semidiscrete central-upwind schemes for hyperbolic conservation laws and Hamilton-Jacobi equations. *Journal of Scientific Computing*, 2002.
- [15] M. Li, F. Guyenne, F. Li, and L. Xu. High order well-balanced CDG-FE methods for shallow water waves by a Green-Naghdi model. *Journal of Computational Mathematics*, 2014.
- [16] S. Gottlieb, C. Shu, and E. Tadmor. Strong stability-preserving high-order time discretization methods. *Society for Industrial and Applied Mathematics*, 2001.
- [17] S. Roberts and C. Zoppou. Explicit schemes for dam-break simulations. *Journal of Hydraulic Engineering*, 129:11–34, 2003.
- [18] S.D. Conte and C. De Boor. *Elementary numerical analysis: An algorithmic approach*. International Series in Pure and Applied Mathematics. McGraw-Hill Inc., New York, 3rd edition, 1980.
- [19] R. Courant, K. Friedrichs, and H. Lewy. On the partial difference equations of mathematical physics. *IBM Journal of Research and Development*, 11(2):215–234, 1967.
- [20] G.A. El, R.H.J. Grimshaw, and N.F. Smyth. Unsteady undular bores in fully nonlinear shallow-water theory. *Physics of Fluids*, 18(2):027104, 2006.

